Drought years in peatland rewetting: Rapid vegetation succession can maintain the net CO_2 sink function

Florian Beyer[1,*], Florian Jansen[2], Gerald Jurasinski[2], Marian Koch[3,†], Birgit Schröder[2], and Franziska Koebsch[2,*]

[1]Geodesy and Geoinformatics, Faculty for Agricultural and Environmental Sciences, Rostock University, 18059 Rostock, Germany
[2]Landscape Ecology, Faculty for Agricultural and Environmental Sciences, Rostock University, 18059 Rostock, Germany
[3]Soil Physics, Faculty for Agricultural and Environmental Sciences, Rostock University, 18059 Rostock, Germany
[†]deceased, 15 April 2020
[*]These authors contributed equally to this work.

Correspondence: florian.beyer@uni-rostock.de

Abstract. Rewetting is a necessary measure to stop CO_2 emissions of degraded peatlands and to restore their natural habitat and C accumulation function. Although the severity and frequency of droughts is predicted to increase as a consequence of climate change, it is not well understood whether such extreme events can jeopardize rewetting measures. The goal of this study was to better understand drought effects on peatland restoration measures. Based on long-term reference records, we investigated

5   anomalies in vegetation dynamics and CO_2 exchange, including ecosystem respiration (R_{eco}) and gross ecosystem productivity (GEP), in a rewetted fen during the extreme European summer drought 2018. Drought-induced vegetation dynamics were derived from remotely sensed data.

Since flooding in 2010, the fen was characterized by a patchy mosaic of open water surfaces and vegetated areas. After years of stagnant vegetation development, drought acted as a trigger event for pioneer species such as *Tephroseris palustris*

10 and *Ranunculus sceleratus* to rapidly close persistent vegetation gaps. The massive spread of vegetation assimilated substantial amounts of CO_2. In 2018, the annual GEP budget increased by 20 % in comparison to average years (2010–2017). R_{eco} increased even by 40 %, but enhanced photosynthetic CO_2 sequestration could compensate for half of the drought-induced increase in respiratory CO_2 release. Altogether, the restored fen remained a net CO_2 sink in the year of drought, though net CO_2 sequestration was lower than in other years.

15 Our study reveals an important regulatory mechanism of restored fens to maintain their net CO_2 sink function even in extremely dry years. Even in times of more frequent climate extremes, fen restoration can create ecosystems resilient to drought. However, further research needs to focus on the long-term effects of such extreme events beyond the actual drought period.

1   Introduction

Peatlands constitute the largest terrestrial C store and exert significant feedback effects on the climate system (Gorham, 1991;

20 Frolking and Roulet, 2007; Yu et al., 2010). Among minerotrophic peatlands (fens) in mid Europe, 90 % have been drained, most of them for agricultural purposes (Pfadenhauer and Grootjans, 1999; Moen et al., 2017). Under drainage, oxgygen avail-

ability initiates a cascade of organic matter breakdown that culminates in peat decomposition (Freeman et al., 2004; Fenner and Freeman, 2011). In this way, drainage turns peatlands from CO_2 sinks to CO_2 sources.

Rewetting is a common measure to restore the natural habitat and C accumulation function of degraded fens. Although
25 rewetting may resume the emissions of methane (CH_4), a strong, yet short-lived greenhouse gas, the resulting climate warming effect is outweighed by the savings of CO_2 emissions in comparison to the previous drainage state (Günther et al., 2020). Therefore, climate mitigation measures in peatlands need to focus primarily on the reduction of the CO_2 source (Tiemeyer et al., 2020). The successful implementation of peatland rewetting can be challenging, as the degradation processes provoked by drainage are largely irreversible. Under intense compaction and decomposition, the peat surface can subside for several
30 decimeters (Leifeld et al., 2011) and rewetted fen areas can easily develop to shallow lakes with average water depths of 20—60 cm (Steffenhagen et al., 2012). Slow or stagnant vegetation development retards the extensive spread of peatland species as prerequisite for CO_2 uptake and C accumulation (Timmermann et al., 2009; Koch et al., 2017). Further, even under flooded conditions, respiratory CO_2 release from peat decomposition can remain high (Franz et al., 2016) as the preceding drainage-rewetting sequence might have increased labile C levels (Freeman et al., 2004; Fenner and Freeman, 2011).

35 Given the importance of hydrological conditions for peat conservation and formation, also meteorological drought can severely impact peatland functioning (Dise, 2009). In analogy to human-induced drainage, drought implies a lowering of the ground water level which may enhance ecosystem respiration (R_{eco}) and peat consumption (Alm et al., 1999; Lund et al., 2012; Koebsch et al., 2013). Further, gross ecosystem productivity (GEP) may decrease as plant stress due to drought limits photosynthetic CO_2 uptake (Shurpali et al., 1995; Arneth et al., 2002; Lafleur et al., 2003; Lund et al., 2012). Altogether, years
40 of drought may turn peatlands from net CO_2 sinks to sources of CO_2 (Lafleur et al., 2003; Lund et al., 2012).

In view of increasing frequency and severity of climatic extreme events (Pachauri et al., 2014), drought has the potential to jeopardize peatland restoration goals (Lavendel, 2003; Harris et al., 2006). However, drought effects have been mostly investigated in near-natural boreal bogs (Shurpali et al., 1995; Alm et al., 1999; Arneth et al., 2002; Lafleur et al., 2003; Lund et al., 2012). As hydrological and vegetation characteristics differ between peatland types, the same drought-related
45 mechanisms may not necessarily occur in fens (Sulman et al., 2010). Even comparisons with pristine fens may be misleading, because the drainage-rewetting sequence irreversibly affects ecosystem functioning of restored fens (Koch et al., 2017). Hence, a better understanding of drought-induced processes in restored fens is needed.

Here, we aim to elucidate the in situ effects of drought on vegetation development and CO_2 exchange in rewetted fens. To this end, we investigated the impact of the extreme summer drought 2018 on a rewetted degraded fen in north eastern Germany.
50 The drought event caused the water level to drop below the ground surface, for the first time since rewetting and therefore provided a good opportunity to investigate our research question. Vegetation development and CO_2 exchange in our particular fen site have been monitored since the rewetting started in 2010, which offers a valueable long-term reference record for the assessment of drought-induced effects. Vegetation dynamics were evaluated both, quantitatively, using the enhanced vegetation index (EVI) derived from MODIS, and, qualitatively, using vegetation mapping derived from multi-sensor data of an unmanned
55 aerial system (UAS). Drought effects on the net CO_2 exchange, including its component fluxes R_{eco}, and GEP were investigated based on a multi-year record of eddy covariance measurements (Montgomery, 1948; Baldocchi, 2003). This interdisciplinary

2

Biogeosciences
Discussions

long-term approach, including ecosystem-scale monitoring of vegetation development and CO_2 exchange, allowed us to track the response mechanisms of a rewetted fen to a severe drought event and to infer insights about the resilience of this novel ecosystem in times of more frequently upcoming climate extremes.

60 ## 2 Methods

2.1 Site description

The study area "Rodewiese" (WGS84: N 54.211°, E 12.178°) is a coastal paludification fen in the nature reserve "Heiligensee und Hütelmoor", located in north eastern Germany (Figure 1). The area has been heavily drained for grassland use since the
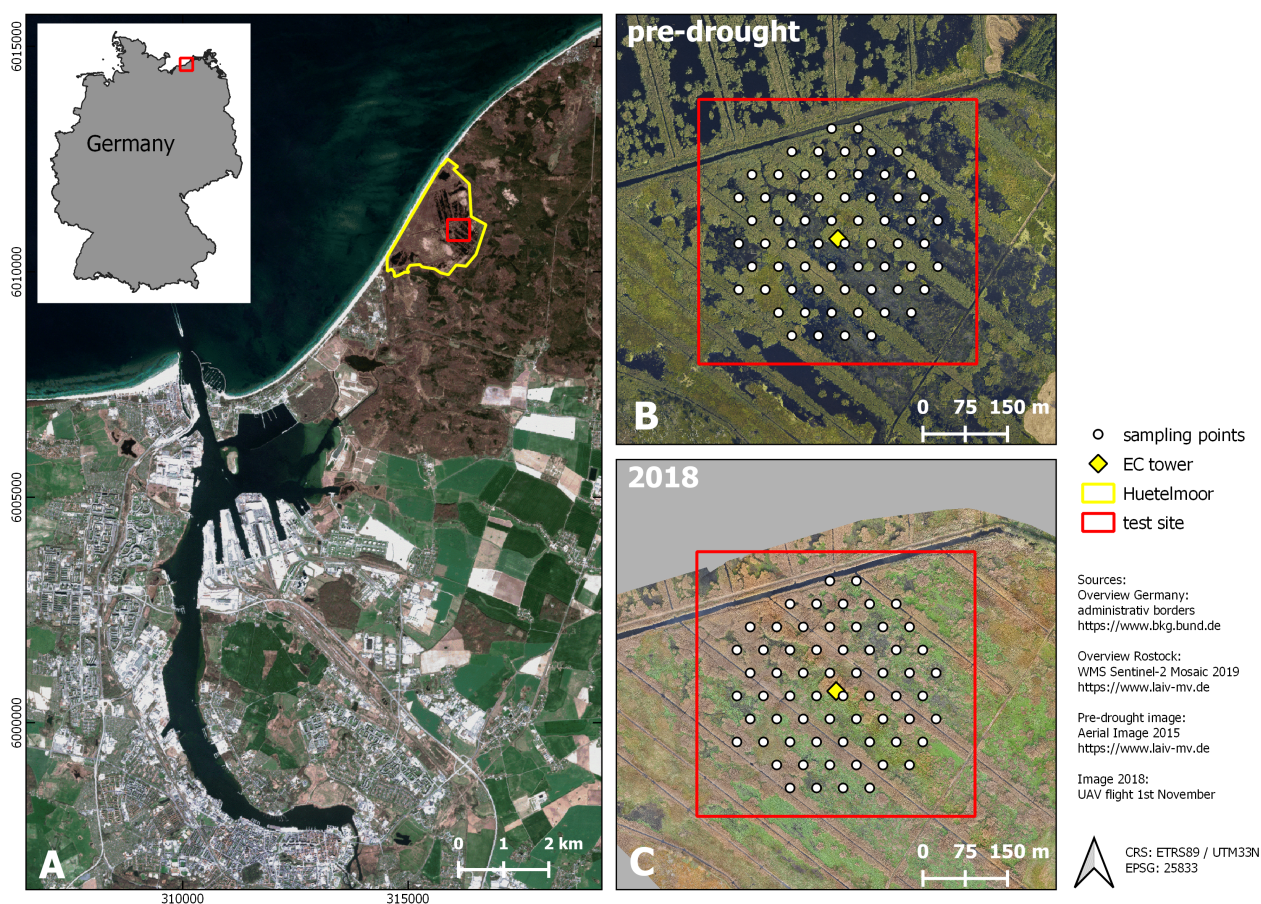

Figure 1. Study site. A: Location (City of Rostock). B (August 2015) and C (November 2018): Aerial photograph with vegetation survey grid. From 2010 to 2017 (pre-drought), the fen was almost permanently inundated. At that time, the canopy consisted of a patchy mosaic of open water and vegetated areas. During the drought 2018, the site fell completely dry, except for the former drainage ditches.

3

1970s with water levels down to 1.6 m below ground. Under drainage, the peat was degraded strongly, and can, nowadays, be described as sapric histosol. In winter 2009/2010, the site was rewetted with the goal to stop peat decomposition and to create a

65 self-regulating ecosystem and water fowl habitat. As a result of rewetting, the site became inundated year-round and the canopy turned to a patchy mosaic of different dominant species and open water areas. Since then, the vegetation was dominated by stands of competitive emergent macrophytes such as Common Reed (*Phragmites australis*) and Lesser-Pond sedge (*Carex acutiformis*) as well as Grey and Sea Club rush (*Schoenoplectus tabernaemontani* and *Bolboschoenus maritimus*). Both of the two latter species present relics of former brackish impact from the near-by Baltic sea. Vegetation patterns were mostly

70 stable in the years following inundation with a slight tendency towards higher patch compactness. Koch et al. (2017) provide a detailed description of the vegetation development of 2011 until 2014.

2.2 Vegetation mapping

2.2.1 Preprocessing of the unmanned aerial system data

Unmanned aerial system data were collected to classify plant composition and distribution of the dominant species. In order to

75 assess the drought effect on vegetation, the changes observed in 2018 were related to the state prior to drought as described in Koch et al. (2017). Accordingly, the study area and processing routines for 2018 were harmonized to the best possible degree with the approach used in Koch et al. (2017). In contrast to Koch et al. (2017) not only normal RGB data and texture indices were available but also additional sensors as well as data types (additional wavelengths and geometrical information) were used.

80 Aerial images were acquired in late autumn (1 November 2018) using an fixed-wing unmanned aerial system (UAS, Sensefly eBee Plus). As the UAS can operate only one camera at a time, high-resolution true color images (SenseFly S.O.D.A, 20 Mpix), multispectral images (Parrot Sequoia, 4x 1.2 Mpix) and thermal images (SenseFly ThermoMap, 0.3 Mpix) were taken during subsequent flights within a time frame where insolation can be considered as stable. The acquired images were then mosaiced with the photogrammetric software Pix4D (Figure B1, appendix B1). The multisensor data set was processed as described in

85 Beyer et al. (2019) and, eventually, consisted of 107 bands: 3 RGB bands, 4 multispectral bands, and 1 thermal band, as well as 1 digital surface model (DSM), 74 spectral and 24 textural indices. The DSM was derived photogrammetrically using RGB color information (Figure B1) and can, due to the flat topography of the study area, be interpreted as plant height proxy. The texture indices were calculated as in Koch et al. (2017) for each RGB band. The 74 spectral indices were selected using the Index Database (www.indexdatabase.de, Henrich et al. (2012, 2009)). The main reason to select such a high number of spectral

90 indices was not only to improve the classification accuracy but especially to get better knowledge of the importance of the specific wavelengths used within the multisensor data set. This approach continues the earlier study from Beyer et al. (2019). All bands, indices and their meaning are listed in Appendix B3 (Table B1). Further, a Python script and an overview of the used indices can be found on github.com/florianbeyer/SpectralIndices.

2.2.2 Vegetation survey

95 Likewise, with the study of Koch et al. (2017), vegetation sampling in 2018 was conducted within an equidistant grid of 64 circular plots, each with a 1m radius (Figure 1). The re-survey was conducted at the end of September and included total plant coverage as well as species coverage (%). Among the 36 species found, only *Phragmites australis*, *Schoenoplectus tabernaemontani*, *Bolboschoenus maritimus*, *Tephroseris palustris*, *Ranunculus sceleratus*, and *Carex acutiformis* were occuring in dominant stands. Here, dominance was defined by (1) the per-plot-abundance and (2) the occurrence frequency across all 64

100 sample points (more than 30 times occurred in 65 plots or more than 50 % occurrence per plot). These six dominant species were, in concert with bare peat and open water, incorporated as surface classes in the following analysis.

2.2.3 Vegetation classification

To classify the vegetation cover, we used the Random Forest (RF, Breiman (2001)) classifier with 500 trees and a minimum branching depth of 2. RF has proven to be a robust and efficient machine learning classification approach in previous remote

105 sensing studies (Beyer et al., 2015; Belgiu and Drăguţ, 2016; Beyer et al., 2019). On the basis of the vegetation mapping, a calibration data set was generated in GIS in order to train the RF. We assessed the performance of the RF model with an independent validation data set. The RF classification algorithm achieved an overall accuracy of 99.84 %. Also, the single class accuracies were high and ranged between 98 and 100 %. In addition, we extracted the importance of every single band in the multisensor data set using the GINI coeffcient (Archer and Kimes, 2008) in order to assess the most important input variables.

110 The results of the importance analysis is summarized in Table B2 (Appendix B3). The classification script can be found at github.com/florianbeyer/RandomForest-Classification.

2.3 CO$_2$ flux processing

Net CO$_2$ exchange was determined with the eddy covariance approach, which provides a continuous time series of half hourly fluxes on ecosystem scale. The setup comprised an open-path infrared gas analyzer (IRGA, LI-7500, LI-COR, Lincoln, NE,

115 USA) measuring CO$_2$ molar density and a three-dimensional sonic anemometer (CSAT3, Campbell Scientific, Logan, UT, USA) measuring wind velocities and sonic temperature. All signals were recorded by a CR3000 Micrologger (Campbell Scientific, Logan, Utah) with a scan rate of 10 Hz. The tower is installed in the middle of the test site (see Figure 1) and has a maximum spatial measuring footprint of 300 m. The main footprint climatology (90 % to the growing season flux), however, happens in a radius of around 200 m (Figure B2, Appendix B2) and was identified in Koebsch et al. (2013).

120 Half-hourly net CO$_2$ fluxes were processed with the software EddyPro version 6.0.0 (LI-COR, Lincoln, NE, USA) using the common corrections for open path eddy covariance set ups. Refer to Koebsch et al. (2013) and Koebsch et al. (2015) for more details on the setup and the complete sequence of flux processing steps.

Data gaps in the CO$_2$ flux time series were filled using artificial neural networks (ANNs, Bishop (1995)) based on the common back propagation algorithm incorporated in the R package neuralnet (R Core Team 2019; Fritsch 2016). Gap filling

125 was conducted in two steps: (1) For small data gaps < 24 hours, we set up several ANNs that predicted half-hourly fluxes

separately for each year. (2) For larger data gaps > 24 hours, we aggregated the data set day-wise and set up a single ANN that encompassed all available measurements from 2009 to 2018. Input variables for all ANNs included air temperature, global radiation, and EVI, as well as fuzzy-transformed variables for time of day and season. A simple architecture comprising one hidden layer and 3–4 nodes proved applicable for all ANNs. Validation of the ANNs with an independent data subset yielded

130   determination coefficients ranging from 0.63–0.83 for half hourly fluxes and 0.77 for daily aggregated fluxes.

The net ecosystem exchange of CO_2 (NEE) was further partitioned into its two component fluxes gross ecosystem productivity (GEP) and ecosystem respiration (R_{eco}, eq. 1).

$$NEE = R_{eco} - GEP \qquad (1)$$

Hereby, GEP represents the photosynthetic sequestration of CO_2 from the atmosphere into the canopy, whilst R_{eco} represents

135   the CO_2 release by autotrophic and heterotrophic respiration into the atmosphere. We partitioned NEE into its component fluxes with an ANN algorithm that predicted R_{eco} from the daily aggregated nighttime fluxes (global radiation threshold < 5 W/m^2). Subsequently, we calculated GEP from the difference between the measured daytime NEE and modeled R_{eco}. Input variables for the ANN included air temperature, water level, EVI, as well as fuzzy-transformed variables for different seasons. The ANN was build from one hidden layer and 4 nodes. Validation of the ANN yielded a determination coefficient for the nighttime

140   fluxes of 0.88.

2.4 Auxiliary data

Meteorological measurements since 2009 were conducted directly at the eddy covariance tower and logged in 30 minute intervals. Measurements included (1) global radiation (Rg), measured with a pyranometer (CMP 3; Kipp & Zonen, Delft, the Netherlands), (2) air temperature (HMP45C, Vaisala, Vantaa, Finland) (3) and precipitation (52203 RM Young). Minor Data

145   gaps were filled with data from a nearby station of the German Weather Service (DWD) in 7.5 km distance to our field station (cdc.dwd.de/portal/ Stations-ID: 4271). DWD weather data were also used for the meteorological long-time reference period 1999–2017.

The water level time series was reconstructed back to 2010 from manual discrete measurements and pressure-compensated automated measurements (Onset U20-001-01 Water Level Data Logger, Onset, Bourne, USA). The final water level time series

150   is referenced to the average elevation height of the fen with positive values indicating water levels above surface.

From the MODIS data products the enhanced vegetation index (EVI) as proxy for plant phenology and vitality was obtained using the NASA AppEEARS tool (lpdaacsvc.cr.usgs.gov/appeears/). EVI values were retrieved from MOD13A1 and MYD13A1 pixel (covering our test site) for the entire time series 2010–2018 congruent with the eddy covariance flux climatology (Figure B2, Appendix B2). EVI allows the assessment of vegetation development on canopy level which fits very well

155   to the footprint of the EC tower in our test site 1. We combined data from both MODIS satellites, Aqua and Terra, and therefore obtained an EVI time series of 8 day intervals. Values were filtered according to pixel reliability and pixel-wise quality assessment and data gaps were subsequently filled by linear interpolation.

Table 1. Annual means and sums of certain climatic and other parameters used in the manuscript from 2010–2018.

Year	Temperature annual mean (°C)	Precipitation annual sum (mm)	Radiation annual sum (kW/m^2)	Water level annual mean (cm)	Enhanced Vegetation Index annual mean
2010	8.1	706	2096.399	36	0.28
2011	9.8	955	2109.110	41	0.25
2012	9.2	490	2103.767	20	0.26
2013	9.4	611	2183.956	24	0.27
2014	10.7	553	2224.981	19	0.28
2015	10.3	611	2223.394	26	0.27
2016	10.1	479	2160.338	25	0.27
2017	10.1	746	2075.759	39	0.27
2018	10.7	457	2369.617	17	0.32

3   Results and Discussion

3.1   Meteorological and hydrological conditions in 2018

160   At the study site, 2018 was among the warmest and sunniest years within the reference period (1999–2018; Figure 2) with only 2003 sharing the same low precipitation sums (457 mm). Hence, 2018 was also the driest year since rewetting of the fen started in 2010. Mean annual temperature amounted to 10.8 °C which was 1 K above the long term average of the reference period and global radiation in 2018 summed up to 2,370 kW m^{-2} which exceeded the long term radiation sum by 213 kW m^{-2}. Total precipitation sum in 2018 was 160 mm below the long term average total (617 mm (Figure 2b).

165   Drought, excessive heat and radiation in 2018 occurred primarily from April to July. During these months, the mean temperature exceeded the long term average April–July temperature (14.0 °) by 1.9 K. The global radiation sum during April–July 2018 exceeded the average radiation sum by 140 kW m^{-2} (long term average: 1,277 kW m^{-2}). Furthermore, precipitation from April to July 2018 summed up to only 111 mm, which is less than half of the rainfall occurring in average years (228 mm). In particular, May 2018 was extraordinarily dry with only 5 mm of rainfall (average May rainfall: 51 mm).

170   The spatially averaged, mean annual water level (Figure 3a and Table 1) in 2018 was 17 cm above surface level (a.s.l.) which is in the lower range of post-rewetting water levels (20–40 cm a.s.l. from 2010–2018). However, meteorological conditions induced a pronounced hydrological variation during the course of 2018. As a result of unusually high precipitation in the previous year (746 mm), water level was still extraordinarily high (0.4 m a.s.l.) until early spring 2018 but decreased rapidly due to rainfall deficit starting in April. Whilst the fen had been permanently inundated since the rewetting in 2010, the water

175   level dropped below ground surface in August 2018. A water level minimum of 0.4 m below surface level (b.s.l.) was met in October.
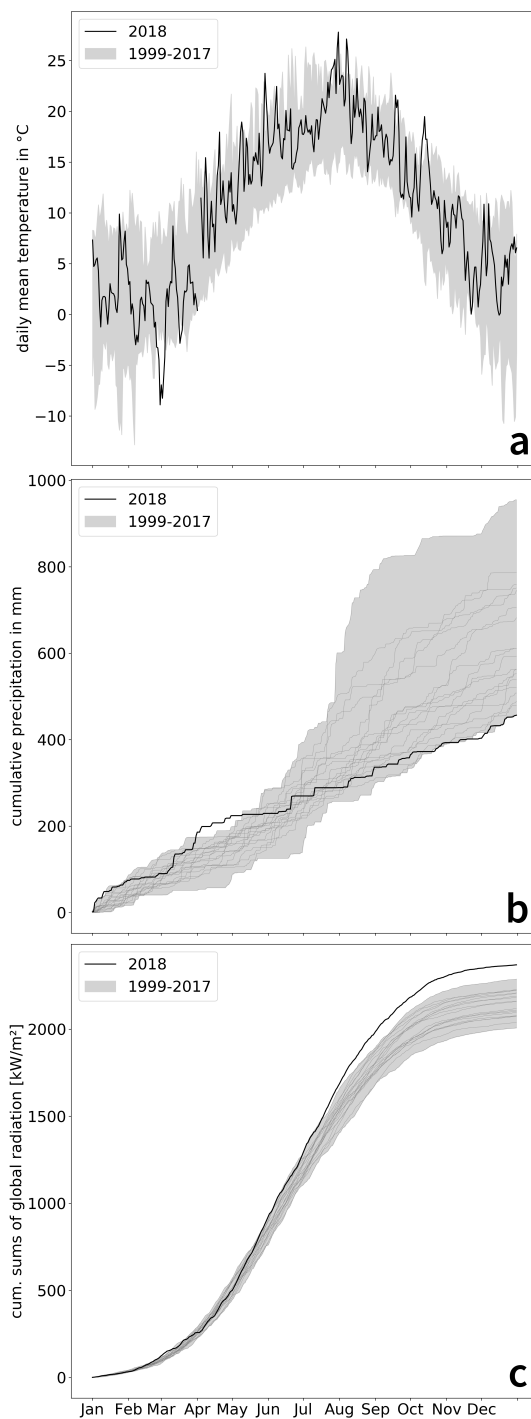
Figure 2. Air temperature (a), cumulative precipitation (b) and cumulative global radiation (c) over the course of the year. Variables are represented as black line for 2018 whereas the grey shading represents the variable range (minimum-maximum) throughout the reference period 1999–2017.
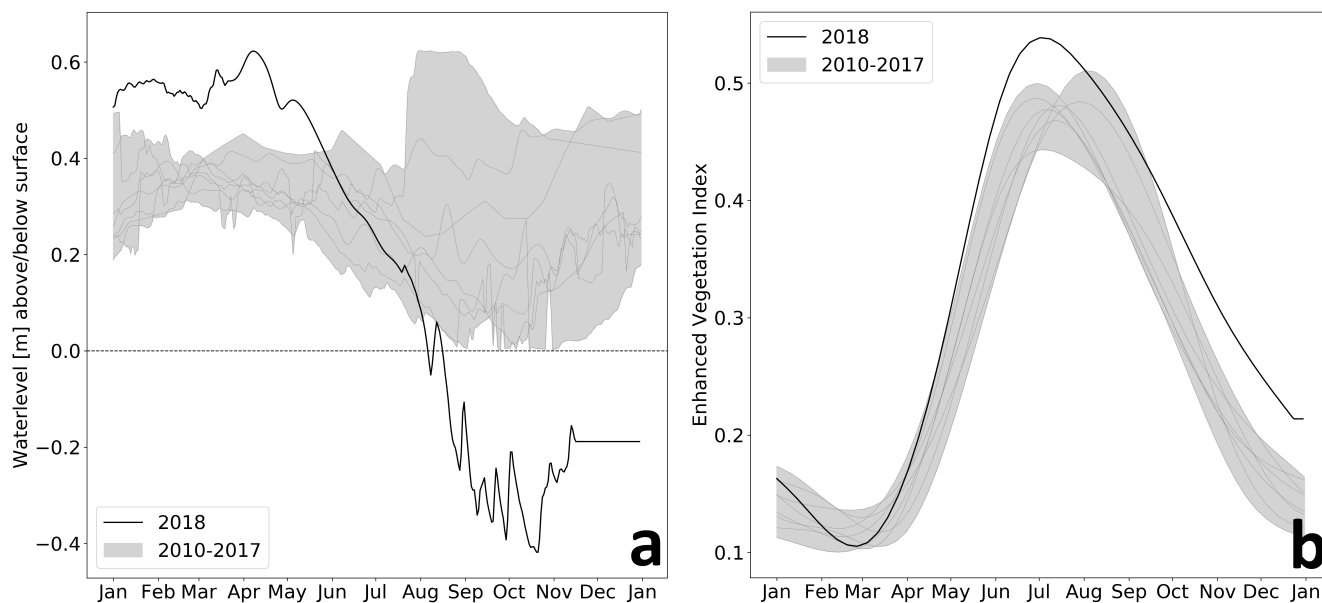
Figure 3. Water level (a) and enhanced vegetation index (b, EVI) over the course of the year. Variables are represented as black line for 2018 whereas the grey shading represents the variable range (minimum-maximum) throughout the reference period 2010–2017.

## 3.2 Vegetation response to drought

3.2.1 Species shift

Rewetting of the fen in 2010 initiated a shift towards flooding resistant species Koch et al. (2017). However, these dynamics were confined only to the first 1–2 years after rewetting, whilst vegetation development stagnated in the following and provided a stable baseline for the investigation of drought effects. In 2014 (Figure 4a), which serves as reference year for the vegetation situation prior to drought, the fen canopy consisted of *Phragmites australis* (47.8 %), *Schoenoplectus tabernaemontani* (21.0 %), open water (20.5 %) *Carex acutiformis* (5.6 %), and *Bolboschoenus maritimus* (5.1 %). Field observations proved these area proportions to remain stable until 2017. With the exception of Phragmites, which constituted the dominant species (areal proportions of 44.4 %), the drought 2018 dramatically changed the species composition of the site (Figure 4b). When rain failed to fall, open water patches dried up completely and were colonized by *Tephroseris palustris* and *Ranunculus sclera-tus*. Both are pioneer species that can rapidly spread along the nutrient-rich shores of dried-up water bodies (Henker et al., 2006). Though of minor abundance in previous years, (Leipe and Leipe, 2017), in 2018, *Tephroseris palustris* and *Ranunculus sceleratus* gained a spatial coverage of 26.6% within a few weeks. The spatial proportion of both *Bolboschoenus maritimus* and *Schoenoplectus tabernaemontani* decreased from 26.1 down to 6.3 % in 2018. In contrast to previous years, when each of these species formed extensive clusters, they now appeared strongly dispersed and were therefore merged into a single veg-etation class. In contrast, the areal coverage of *Carex acutiformis*, a species adapted to moist conditions, increased from 5.6

to 17.3 %. Hence, after years of stagnation, drought changed the species composition of the fen within weeks: Dried-up open water patches served as habitat for fast-growing pioneer plants, but also the established vegetation responded with substantial withdrawal of flooding-adapted species and a spread of species adapted to moderate moisture.
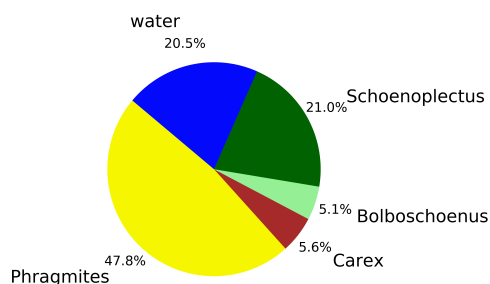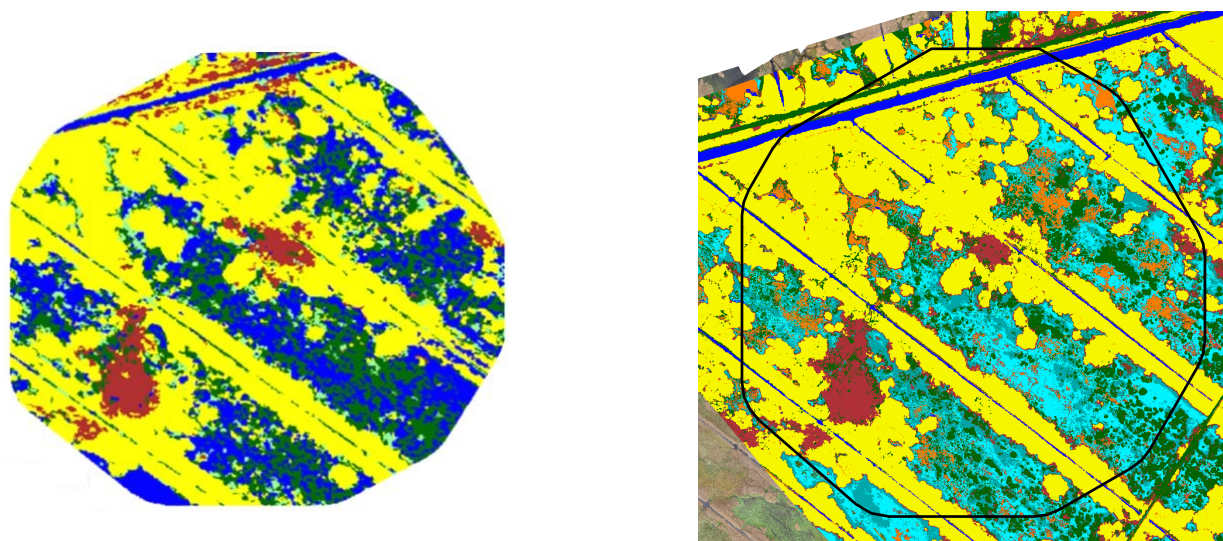
(a) Vegetation composition 2014.
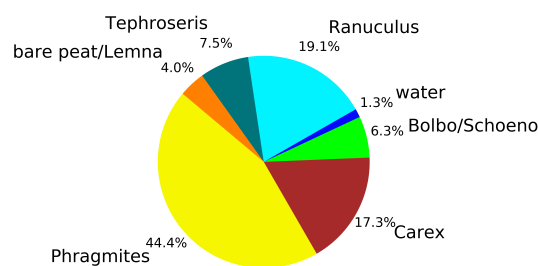
(b) Vegetation composition 2018.

Figure 4. Vegetation composition in 2014 (4a) as presented in Koch et al. (2017) and after the drought in 2018 (4b, black border marks study site extend of Koch et al. (2017)).

195

3.2.2 Seasonal dynamics

Vegetation dynamics, expressed by the EVI, were exceptional in 2018. The EVI increased rapidly from a comparatively low initial value of 0.1 in February/March to a new maximum of 0.53 at the start of July. The steep spring-time rise and the high summer peak in EVI can most likely be attributed to the rapid growth of the established vegetation which was triggered by high temperatures and radiation supply from April on. However, in comparison to other years, EVI decreased early at the beginning of July 2018, which marked the onset of drought-related changes in canopy reflectance when water level dropped below 0.2 m

10

a.s.l. At that time, extensive vegetation areas were already affected by drought, even if the spatially averaged water level was still relatively high. During the following months, the subsequent downward trend in EVI slowed down considerably. From September 2018 on, EVI was distinctively higher than normally, indicating an extension of the growing season until late in

205   the year. Mean annual EVI of 0.32 in 2018 compared to the mean of time series 2010–2017 0.27 (std = 0.009) supports this conclusion (Table 1).

3.3   Response of CO_2 exchange to drought

The restored fen site is highly productive with substantial rates of GEP and R_{eco} (Koebsch et al., 2013). Despite strong inter-annual variation, the fen has acted as net CO_2 sink since rewetting with average NEE budgets of -0.70 kg m^{-2} a^{-1} (Koebsch

210   et al., 2013). New record levels of R_{eco} and GEP were reached in 2018 (Figure 5a and 5b): The annual R_{eco} budget totalled 3.22 kg CO_2 m^{-2} and exceeded the post-rewetting average by 0.93 kg m^{-2}. Further, with -3.61 kg CO_2 m^{-2} total annual GEP exceeded the average photosynthetic CO_2 uptake by 0.63 kg m^{-2}. Hence, in 2018 the fen remained a net CO_2 sink, though net CO_2 sequestration was 0.30 kg m^{-2} lower than in average post-rewetting years.

NEE and its component fluxes marked seasonal dynamics including a decoupling of GEP and R_{eco} when drought took

215   effect from July 2018 on (Figure 5c). Before July, daily R_{eco} and GEP sums were in the upper range of normal years. This is most likely due to high temperatures and radiation supply which fostered efficient growth of the established vegetation. As the rise in C assimilation outweighed the increase in respiratory CO_2 release, the first weeks in the growing season 2018 also exhibited comparatively high rates of net CO_2 uptake. GEP peaked at -37 g CO_2 m^{-2} d^{-1} in June/July which coincided with the maximum EVI. Following this peak, photosynthetic CO_2 uptake decreased substantially, which was likely driven by the

220   onset of drought-induced stress for the established vegetation. At the same time, R_{eco} maintained its upward trend and reached a new record of 25 g CO_2 m^{-2} d^{-1} at the end of July. R_{eco} remained on this plateau for the following two months, reflecting a persistent CO_2 loss due to both, peat and plant decomposition. In normal years, the fen smoothly shifts from being a net CO_2 sink to a net CO_2 source at the end of the growing season. The dry spell in summer 2018, however, caused a rapid switch from net CO_2 sink to CO_2 neutrality already in July. After the drought-related decline in July 2018, GEP increased again in August.

225   This 2nd peak in GEP coincided with the observed colonization of dried-up areas by *Tephroseris palustris* and *Ranunculus sceleratus*. Biomass accumulation through the massive spread of these species held GEP rates high until late in the growing season.

4   Drought response mechanisms of restored fens

Pristine peatlands are adaptive systems characterized by quasi-stable equilibrium states and feature resilience mechanisms to

230   cope with drought to a certain extent (Dise, 2009). The ecohydrology of intact peat is characterized by its large water holding capacity and its capillary wicking processes (Ingram, 1987; Lapen et al., 2000). Whilst these present efficient regulation mechanism to buffer short-term dry spells, persistent drought or increasing drought frequency can also induce shifts in vegetation and C regime (Couwenberg and Joosten, 1999; Couwenberg et al., 2008). In mires, drought can induce changes from low-phenolic
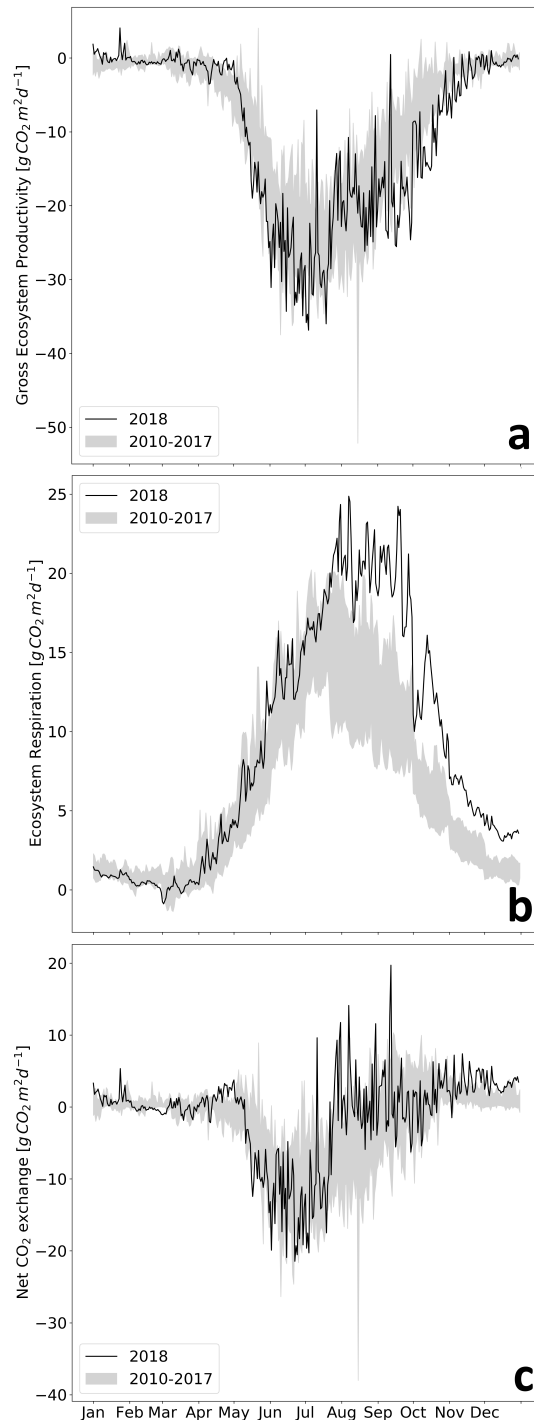
Figure 5. Component fluxes GEP (a) and R$_{eco}$ of NEE (c) over the course of the year. Variables are represented as black line for 2018 whereas the grey shading represents the variable range (minimum-maximum) throughout the reference period 2010–2017.

Sphagnum/herbs towards phenol-rich shrub vegetation which increases C sequestration and protects soil C (Riutta et al., 2007;

235 Limpens et al., 2008; Wang et al., 2015). Drought can even trigger abrupt episodes of habitat conversion, which are essential for the succession trajectory of peatlands. Such drought-induced state-shifts are known for kettle peatland development and are associated with greatly increased C accumulation rates (Ireland et al., 2012).

Analogue climate-feedback mechanisms cannot be anticipated for degraded restored fens, where catchment hydrology, soil and trophic conditions as well as propagule availability have been subject to irreversible change (van Diggelen et al., 2006;

240 Klimkowska et al., 2010). Here, we describe a distinct response mechanism of such newly created systems to severe drought: Sinking water levels exposed bare spots, that were rapidly colonized by pioneer species. Hence, after years of stagnant vegetation development, drought acted as a trigger event to close persistent vegetation gaps. During the build-up of new biomass, substantial amounts of CO_2 were sequestered which overcompensated for the drought-induced decline of photosynthetic CO_2 uptake by the established vegetation. On an annual basis, enhanced GEP offset half of the drought-induced increase in R_{eco}.

245 Therefore, the restored fen maintained its net CO_2 sink function even in such a year of extreme drought.

Further, our study shows, how drought-induced founding effects can give impetus to overcome stagnant vegetation succession of rewetted fens, the canopies of which are often interspersed by more or less extended open water patches where vegetation cannot take root (Steffenhagen et al., 2012; Matthes et al., 2014; Franz et al., 2016). However, the relevance of drought-induced founding events for the long-term succession of restored fens will rely on the capability of the newly formed

250 vegetation to gain a lasting foothold in these systems. Dependent on whether these pioneer species can cope with the recurrent water level rise (Koch et al., 2017), they will contribute to the ecosystems C budget in one way or the other and could initiate silting processes that set the stage for subsequent peat-forming vegetation.

Clearly, further long-term observations are needed to comprehensively elucidate the aftereffects of drought for the development of rewetted fens. Though, in practice, it is difficult to unravel such aftereffects of past events from contemporary

255 influences. For example, we could still observe the presence of *Tephroseris palustris*, despite the resuming water level rise in the year after the drought. However since the majority of the resupplied water originated from an episodic brackish water intrusion event in January 2019, we cannot generalize the observations from 2019 to common freshwater fens. Although our observations are confined to the year of drought, it is conceivable, that such extreme events initiate distinct carry-over effects that extend beyond the actual drought period and can set the course for the future development of restored fens and their C

260 cycle.

Code availability. Both, the classification script and the script to calculate spectral indices can be found at github.com/florianbeyer/RandomForestClassification and github.com/florianbeyer/SpectralIndices.

Appendix A: ORCID IDs

Florian Beyer: 0000-0002-9203-320X

Franziska Koebsch: 0000-0003-1045-7680

Gerald Jursinski: 0000-0002-6248-9388

Florian Jansen: 0000-0002-0331-5185

265 ## Appendix B: Supplementary material
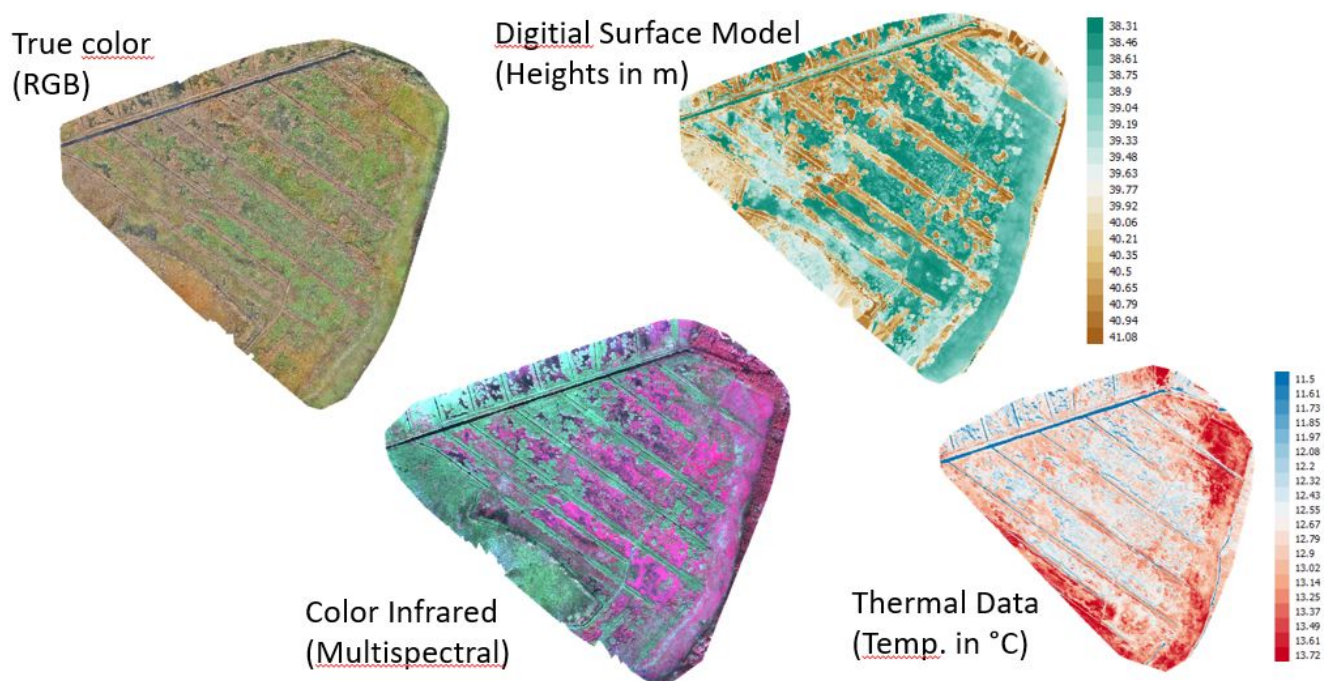
B1 UAS data sets

Figure B1. True color, multispectral (band combination: near infrared|red|green), digital surface model and thermal orthomosaic of the multisensor UAS data.
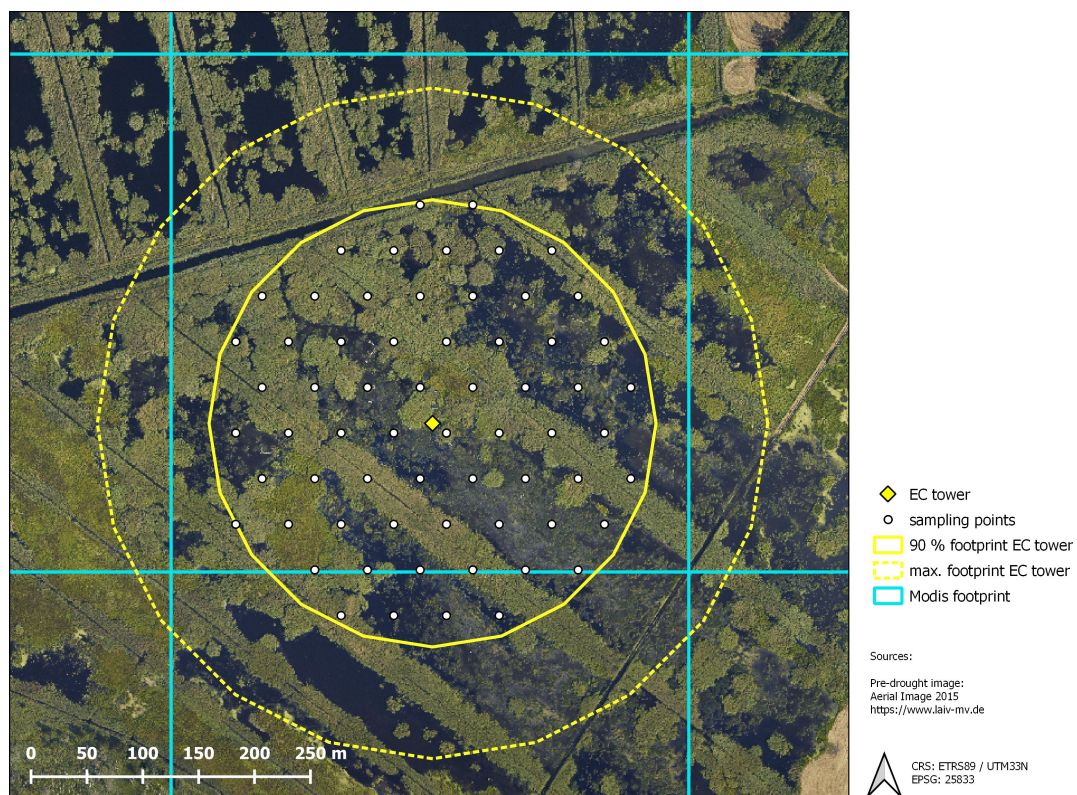
B2 Modis footprint

Figure B2. Spatial comparison of the different data, sampling points, Eddy Covariance (EC) tower footprint and Modis' ground sampling distance.

B3 Bands of the Multisensor data set and its importances for classification

Table B1. Multisensor data set consits of 107 bands. All indices are described in github.com/florianbeyer/SpectralIndices.

No.	Band name	Type/Meaning	Data from	Derived from	No.	Band name	Type/Meaning	Data from	Derived from
1	RGB1	Blue	RGB Sensor		55	fe3	Spectral Index		Multispectral Sensor
2	RGB2	Green	RGB Sensor		56	gemi	Spectral Index		Multispectral Sensor
3	RGB3	Red	RGB Sensor		57	gndvi	Spectral Index		Multispectral Sensor
4	MS1	Green	Multispectral Sensor		58	osavi1	Spectral Index		Multispectral Sensor
5	MS2	Red	Multispectral Sensor		59	osavi2	Spectral Index		Multispectral Sensor
6	MS3	Red Edge	Multispectral Sensor		60	pvr	Spectral Index		Multispectral Sensor
7	MS4	Near Infrared	Multispectral Sensor		61	rdvi	Spectral Index		Multispectral Sensor
8	DSM	Digital Surface Model (DSM)		RGB Sensor	62	rededge2	Spectral Index		Multispectral Sensor
9	th_index	Thermal	Thermal Sensor		63	savi	Spectral Index		Multispectral Sensor
10	ngrdi	Spectral Index		RGB Sensor	64	sbl	Spectral Index		Multispectral Sensor
11	tgi	Spectral Index		RGB Sensor	65	spvi	Spectral Index		Multispectral Sensor
12	vari	Spectral Index		RGB Sensor	66	tc_gvimss	Spectral Index		Multispectral Sensor
13	exg	Spectral Index		RGB Sensor	67	tc_nsimss	Spectral Index		Multispectral Sensor
14	gcc	Spectral Index		RGB Sensor	68	tc_sbimss	Spectral Index		Multispectral Sensor
15	gli	Spectral Index		RGB Sensor	69	tc_yvimss	Spectral Index		Multispectral Sensor
16	ari	Spectral Index		Multispectral Sensor	70	tcari	Spectral Index		Multispectral Sensor
17	arvi2	Spectral Index		Multispectral Sensor	71	tcari_osavi	Spectral Index		Multispectral Sensor
18	atsavi	Spectral Index		Multispectral Sensor	72	tcari2	Spectral Index		Multispectral Sensor
19	avi	Spectral Index		Multispectral Sensor	73	tci	Spectral Index		Multispectral Sensor
20	bri	Spectral Index		Multispectral Sensor	74	tvi	Spectral Index		Multispectral Sensor
21	ccci	Spectral Index		Multispectral Sensor	75	varirededge	Spectral Index		Multispectral Sensor
22	chlgreen	Spectral Index		Multispectral Sensor	76	wdrvi	Spectral Index		Multispectral Sensor
23	chlrededge	Spectral Index		Multispectral Sensor	77	ndrdi	Spectral Index		Multispectral Sensor
24	cigreen	Spectral Index		Multispectral Sensor	78	ndre	Spectral Index		Multispectral Sensor
25	cirededge	Spectral Index		Multispectral Sensor	79	ndvi	Spectral Index		Multispectral Sensor
26	ctvi	Spectral Index		Multispectral Sensor	80	nli	Spectral Index		Multispectral Sensor
27	cvi	Spectral Index		Multispectral Sensor	81	normg	Spectral Index		Multispectral Sensor
28	datt1	Spectral Index		Multispectral Sensor	82	normnir	Spectral Index		Multispectral Sensor
29	datt4	Spectral Index		Multispectral Sensor	83	normr	Spectral Index		Multispectral Sensor
30	ddn	Spectral Index		Multispectral Sensor	84	band1_Energy	Texture Index		RGB Sensor
31	diff1	Spectral Index		Multispectral Sensor	85	band1_Entropy	Texture Index		RGB Sensor
32	diff2	Spectral Index		Multispectral Sensor	86	band1_Correlation	Texture Index		RGB Sensor
33	dvimss	Spectral Index		Multispectral Sensor	87	band1_InverseDifferenceMoment	Texture Index		RGB Sensor
34	gosavi	Spectral Index		Multispectral Sensor	88	band1_Inertia	Texture Index		RGB Sensor
35	grndvi	Spectral Index		Multispectral Sensor	89	band1_ClusterShade	Texture Index		RGB Sensor
36	lai	Spectral Index		Multispectral Sensor	90	band1_ClusterProminence	Texture Index		RGB Sensor
37	lci	Spectral Index		Multispectral Sensor	91	band1_HaralickCorrelation	Texture Index		RGB Sensor
38	logr	Spectral Index		Multispectral Sensor	92	band2_Energy	Texture Index		RGB Sensor
39	maccioni	Spectral Index		Multispectral Sensor	93	band2_Entropy	Texture Index		RGB Sensor
40	mari	Spectral Index		Multispectral Sensor	94	band2_Correlation	Texture Index		RGB Sensor
41	mcari	Spectral Index		Multispectral Sensor	95	band2_InverseDifferenceMoment	Texture Index		RGB Sensor
42	mcari_mtvi2	Spectral Index		Multispectral Sensor	96	band2_Inertia	Texture Index		RGB Sensor
43	mcari_osavi	Spectral Index		Multispectral Sensor	97	band2_ClusterShade	Texture Index		RGB Sensor
44	mcari1	Spectral Index		Multispectral Sensor	98	band2_ClusterProminence	Texture Index		RGB Sensor
45	mcari2	Spectral Index		Multispectral Sensor	99	band2_HaralickCorrelation	Texture Index		RGB Sensor
46	mgvi	Spectral Index		Multispectral Sensor	100	band3_Energy	Texture Index		RGB Sensor
47	mnsi	Spectral Index		Multispectral Sensor	101	band3_Entropy	Texture Index		RGB Sensor
48	msavi	Spectral Index		Multispectral Sensor	102	band3_Correlation	Texture Index		RGB Sensor
49	msbi	Spectral Index		Multispectral Sensor	103	band3_InverseDifferenceMoment	Texture Index		RGB Sensor
50	msr670	Spectral Index		Multispectral Sensor	104	band3_Inertia	Texture Index		RGB Sensor
51	mtvi2	Spectral Index		Multispectral Sensor	105	band3_ClusterShade	Texture Index		RGB Sensor
52	myvi	Spectral Index		Multispectral Sensor	106	band3_ClusterProminence	Texture Index		RGB Sensor
53	evi2	Spectral Index		Multispectral Sensor	107	band3_HaralickCorrelation	Texture Index		RGB Sensor
54	evi22	Spectral Index		Multispectral Sensor					

Biogeosciences
Discussions

Table B2. All bands of the multisensor data set orderd by the GINI coefficient. The higher the GINI the more important is the band for the Random Forest classification.

No.	Band	Gini	Gini (%)	c. Gini	No.	Band	Gini	Gini (%)	cumulative Gini
8	DSM	0.06415	6.4	6.4	63	savi	0.00618	0.6	85.0
35	grndvi	0.03760	3.8	10.2	100	band3_Energy	0.00596	0.6	85.6
82	normnir	0.03268	3.3	13.4	85	band1_Entropy	0.00560	0.6	86.1
17	arvi2	0.02773	2.8	16.2	106	band3_ClusterProminence	0.00556	0.6	86.7
50	msr670	0.02674	2.7	18.9	96	band2_Inertia	0.00551	0.6	87.2
74	tvi	0.02510	2.5	21.4	45	mcari2	0.00539	0.5	87.8
38	logr	0.02499	2.5	23.9	87	band1_InverseDifferenceMoment	0.00522	0.5	88.3
76	wdrvi	0.02460	2.5	26.4	43	mcari_osavi	0.00522	0.5	88.8
52	myvi	0.02302	2.3	28.7	93	band2_Entropy	0.00517	0.5	89.3
49	msbi	0.02271	2.3	30.9	54	evi22	0.00498	0.5	89.8
40	mari	0.02140	2.1	33.1	95	band2_InverseDifferenceMoment	0.00492	0.5	90.3
30	ddn	0.02102	2.1	35.2	48	msavi	0.00486	0.5	90.8
5	MS2	0.02093	2.1	37.3	80	nli	0.00485	0.5	91.3
79	ndvi	0.02086	2.1	39.4	102	band3_Correlation	0.00485	0.5	91.8
26	ctvi	0.01867	1.9	41.2	53	evi2	0.00478	0.5	92.3
34	gosavi	0.01826	1.8	43.0	101	band3_Entropy	0.00477	0.5	92.7
67	tc_nsimss	0.01819	1.8	44.9	84	band1_Energy	0.00456	0.5	93.2
64	sbl	0.01775	1.8	46.6	66	tc_gvimss	0.00443	0.4	93.6
83	normr	0.01750	1.7	48.4	29	datt4	0.00435	0.4	94.1
47	mnsi	0.01665	1.7	50.1	36	lai	0.00432	0.4	94.5
31	diff1	0.01630	1.6	51.7	44	mcari1	0.00432	0.4	94.9
68	tc_sbimss	0.01529	1.5	53.2	81	normg	0.00386	0.4	95.3
75	varirededge	0.01527	1.5	54.7	104	band3_Inertia	0.00370	0.4	95.7
70	tcari	0.01515	1.5	56.3	65	spvi	0.00367	0.4	96.0
7	MS4	0.01454	1.5	57.7	11	tgi	0.00301	0.3	96.3
22	chlgreen	0.01404	1.4	59.1	98	band2_ClusterProminence	0.00291	0.3	96.6
60	pvr	0.01399	1.4	60.5	4	MS1	0.00289	0.3	96.9
6	MS3	0.01375	1.4	61.9	105	band3_ClusterShade	0.00275	0.3	97.2
55	fe3	0.01319	1.3	63.2	90	band1_ClusterProminence	0.00268	0.3	97.5
33	dvimss	0.01283	1.3	64.5	32	diff2	0.00257	0.3	97.7
24	cigreen	0.01272	1.3	65.8	14	gcc	0.00246	0.2	98.0
19	avi	0.01267	1.3	67.0	15	gli	0.00240	0.2	98.2
9	th_index	0.01096	1.1	68.1	89	band1_ClusterShade	0.00222	0.2	98.4
27	cvi	0.01083	1.1	69.2	59	osavi2	0.00169	0.2	98.6
57	gndvi	0.00977	1.0	70.2	10	ngrdi	0.00160	0.2	98.8
71	tcari_osavi	0.00975	1.0	71.2	86	band1_Correlation	0.00145	0.1	98.9
77	ndrdi	0.00957	1.0	72.1	12	vari	0.00144	0.1	99.1
107	band3_HaralickCorrelation	0.00896	0.9	73.0	69	tc_yvimss	0.00142	0.1	99.2
58	osavi1	0.00885	0.9	73.9	94	band2_Correlation	0.00097	0.1	99.3
56	gemi	0.00879	0.9	74.8	97	band2_ClusterShade	0.00085	0.1	99.4
91	band1_HaralickCorrelation	0.00874	0.9	75.7	78	ndre	0.00070	0.1	99.4
103	band3_InverseDifferenceMoment	0.00838	0.8	76.5	25	cirededge	0.00062	0.1	99.5
73	tci	0.00816	0.8	77.3	23	chlrededge	0.00059	0.1	99.6
16	ari	0.00811	0.8	78.1	72	tcari2	0.00058	0.1	99.6
18	atsavi	0.00773	0.8	78.9	21	ccci	0.00051	0.1	99.7
99	band2_HaralickCorrelation	0.00772	0.8	79.7	61	rdvi	0.00051	0.1	99.7
51	mtvi2	0.00727	0.7	80.4	37	lci	0.00051	0.1	99.8
20	bri	0.00686	0.7	81.1	62	rededge2	0.00050	0.1	99.8
42	mcari_mtvi2	0.00682	0.7	81.8	28	datt1	0.00046	0.0	99.9
88	band1_Inertia	0.00660	0.7	82.4	39	maccioni	0.00038	0.0	99.9
92	band2_Energy	0.00659	0.7	83.1	3	RGB3	0.00035	0.0	100.0
41	mcari	0.00643	0.6	83.7	13	exg	0.00029	0.0	100.0
46	mgvi	0.00627	0.6	84.3	1	RGB1	0.00011	0.0	100.0
					2	RGB2	0.00009	0.0	100.0

Author contributions.   Franziska Koebsch conceived the study. Florian Beyer and Franziska Koebsch carried out the experiments and wrote
270   the manuscript. Florian Jansen and Gerald Jurasinski revised the manuscript and contributed with helpful comments. Marian Koch revised
the manuscript and conducted the first studies on which the manuscript is based. Birgit Schröder carried out the vegetation mapping and
helped with botanical issues.

Competing interests.   The authors declare that they have no conflicts of interest.

References

Alm, J., Schulman, L., Walden, J., Nykänen, H., Martikainen, P., and Silvola, J.: Carbon balance of a boreal bog during a year with an exceptionally dry summer, Ecology, 80, 161–174, https://doi.org/10.1890/0012-9658(1999)080[0161:CBOABB]2.0.CO;2, https://esajournals.onlinelibrary.wiley.com/doi/abs/10.1890/0012-9658%281999%29080%5B0161%3ACBOABB%5D2.0.CO%3B2, 1999.

285 Archer, K. J. and Kimes, R. V.: Empirical characterization of random forest variable importance measures, Computational Statistics & Data Analysis, 52, 2249–2260, https://doi.org/10.1016/j.csda.2007.08.015, http://linkinghub.elsevier.com/retrieve/pii/S0167947307003076, 2008.

Arneth, A., Kurbatova, J., Kolle, O., Shibistova, O. B., Lloyd, J., Vygodskaya, N. N., and Schulze, E.-D.: Comparative ecosystem–atmosphere exchange of energy and mass in a European Russian and a central Siberian bog II. Interseasonal and interannual variability of CO_2 fluxes,

290 Tellus B: Chemical and Physical Meteorology, 54, 514–530, https://doi.org/10.3402/tellusb.v54i5.16684, https://www.tandfonline.com/doi/full/10.3402/tellusb.v54i5.16684, 2002.

Baldocchi, D. D.: Assessing the eddy covariance technique for evaluating carbon dioxide exchange rates of ecosystems: past, present and future, Global Change Biology, 9, 479–492, https://doi.org/10.1046/j.1365-2486.2003.00629.x, http://doi.wiley.com/10.1046/j.1365-2486.2003.00629.x, 2003.

295 Belgiu, M. and Drăguţ, L.: Random forest in remote sensing: A review of applications and future directions, ISPRS Journal of Photogrammetry and Remote Sensing, 114, 24–31, https://doi.org/10.1016/j.isprsjprs.2016.01.011, https://linkinghub.elsevier.com/retrieve/pii/S0924271616000265, 2016.

Beyer, F., Jarmer, T., and Siegmann, B.: Identification of Agricultural Crop Types in Northern Israel using Multitemporal RapidEye Data, Photogrammetrie - Fernerkundung - Geoinformation, 2015, 21–32, https://doi.org/10.1127/pfg/2015/0249, https://doi.org/10.1127/pfg/2015/0249, 2015.

300 Beyer, F., Jurasinski, G., Couwenberg, J., and Grenzdörffer, G.: Multisensor data to derive peatland vegetation communities using a fixed-wing unmanned aerial vehicle, International Journal of Remote Sensing, 00, 1–23, https://doi.org/10.1080/01431161.2019.1580825, https://doi.org/10.1080/01431161.2019.1580825, 2019.

Bishop, C. M.: Neural Networks for Pattern Recognition, Oxford University Press, Inc., New York, NY, USA, 1995.

305 Breiman, L.: Random Forests, Machine Learning, 45, 5–32, https://doi.org/10.1023/A:1010933404324, https://doi.org/10.1023/A:1010933404324, 2001.

Couwenberg, J. and Joosten, H.: Pools as missing links: the role of nothing in the being of mires, in: Patterned mires and mire pools - Origin and development; flora and fauna, edited by Standen, V., Tallis, J., and Meade, R., pp. 87–102, 1999.

Couwenberg, J., Augustin, J., Michaelis, D., Wichtmann, W., and Joosten, H.: Entwicklung von Grundsätzen für eine Bewertung von
310 Niedermooren hinsichtlich ihrer Klimarelevanz. Studie im Auftrag des Ministerium für Landwirtschaft und Naturschutz Mecklenburg-Vorpommern, Tech. rep., 2008.

Dise, N. B.: Peatland Response to Global Change, Science, 326, 810–811, https://doi.org/10.1126/science.1174268, http://www.sciencemag.org/cgi/doi/10.1126/science.1174268, 2009.

Fenner, N. and Freeman, C.: Drought-induced carbon loss in peatlands, Nature Geoscience, 4, 895–900, https://doi.org/10.1038/ngeo1323,
315 http://www.nature.com/articles/ngeo1323, 2011.

Franz, D., Koebsch, F., Larmanou, E., Augustin, J., and Sachs, T.: High net CO&lt;sub&gt;2&lt;/sub&gt; and CH&lt;sub&gt;4&lt;/sub&gt; release at a eutrophic shallow lake on a formerly drained fen, Biogeosciences, 13, 3051–3070, https://doi.org/10.5194/bg-13-3051-2016, https://www.biogeosciences.net/13/3051/2016/, 2016.

Freeman, C., Ostle, N., Fenner, N., and Kang, H.: A regulatory role for phenol oxidase during decomposition in peatlands, Soil Biology and Biochemistry, 36, 1663–1667, https://doi.org/10.1016/j.soilbio.2004.07.012, https://linkinghub.elsevier.com/retrieve/pii/S0038071704002044, 2004.

Frolking, S. and Roulet, N. T.: Holocene radiative forcing impact of northern peatland carbon accumulation and methane emissions, Global Change Biology, 13, 1079–1088, https://doi.org/10.1111/j.1365-2486.2007.01339.x, http://doi.wiley.com/10.1111/j.1365-2486.2007.01339.x, 2007.

Gorham, E.: Northern Peatlands: Role in the Carbon Cycle and Probable Responses to Climatic Warming, Ecological Applications, 1, 182–195, https://doi.org/10.2307/1941811, http://doi.wiley.com/10.2307/1941811, 1991.

Günther, A., Barthelmes, A., Huth, V., Joosten, H., Jurasinski, G., Koebsch, F., and Couwenberg, J.: Prompt rewetting of drained peatlands reduces climate warming despite methane emissions, Nature Communications, 11, 1644, https://doi.org/10.1038/s41467-020-15499-z, http://www.nature.com/articles/s41467-020-15499-z, 2020.

Harris, J. A., Hobbs, R. J., Higgs, E., and Aronson, J.: Ecological Restoration and Global Climate Change, Restoration Ecology, 14, 170–176, https://doi.org/10.1111/j.1526-100X.2006.00136.x, http://doi.wiley.com/10.1111/j.1526-100X.2006.00136.x, 2006.

Henker, H., Fukarek, F., and Berg, C.: Flora von Mecklenburg-Vorpommern: Farn- und Blütenpflanzen, Weissdorn-Verlag, Jena, 2006.

Henrich, V., Jung, A., Götze, C., Sandow, C., Thürkow, D., and Gläßer, C.: Development of an online indices database: Motivation, concept and implementation, in: 6th EARSeL Imaging Spectroscopy SIG Workshop Innovative Tool for Scientific and Commercial Environment Applications, http://earsel6th.tau.ac.il/~earsel6/CD/PDF/earsel-PROCEEDINGS/3064Henrich.pdf, 2009.

Henrich, V., Krauss, G., Götze, C., and Sandow, C.: IDB - www.indexdatabase.de, Entwicklung einer Datenbank für Fernerkundungsindizes, in: AK Fernerkundung, https://www.indexdatabase.de/info/credits.php, 2012.

Ingram, H. A. P.: Ecohydrology of Scottish peatlands, Transactions of the Royal Society of Edinburgh: Earth Sciences, 78, 287–296, https://doi.org/10.1017/S0263593300011226, https://www.cambridge.org/core/product/identifier/S0263593300011226/type/journal_article, 1987.

Ireland, A. W., Booth, R. K., Hotchkiss, S. C., and Schmitz, J. E.: Drought as a Trigger for Rapid State Shifts in Kettle Ecosystems: Implications for Ecosystem Responses to Climate Change, Wetlands, 32, 989–1000, https://doi.org/10.1007/s13157-012-0324-6, http://link.springer.com/10.1007/s13157-012-0324-6, 2012.

Klimkowska, A., Van Diggelen, R., Grootjans, A. P., and Kotowski, W.: Prospects for fen meadow restoration on severely degraded fens, Perspectives in Plant Ecology, Evolution and Systematics, 12, 245–255, https://doi.org/10.1016/j.ppees.2010.02.004, https://linkinghub.elsevier.com/retrieve/pii/S143383191000020X, 2010.

Koch, M., Koebsch, F., Hahn, J., and Jurasinski, G.: From meadow to shallow lake: Monitoring secondary succession in a coastal fen after rewetting by flooding based on aerial imagery and plot data, Mires and Peat, 19, 1–17, https://doi.org/10.19189/MaP.2015.OMB.188, http://www.mires-and-peat.net/,, 2017.

Koebsch, F., Glatzel, S., Hofmann, J., Forbrich, I., and Jurasinski, G.: CO 2 exchange of a temperate fen during the conversion from moderately rewetting to flooding, Journal of Geophysical Research: Biogeosciences, 118, 940–950, https://doi.org/10.1002/jgrg.20069, http://doi.wiley.com/10.1002/jgrg.20069, 2013.

Koebsch, F., Jurasinski, G., Koch, M., Hofmann, J., and Glatzel, S.: Controls for multi-scale temporal variation in ecosystem methane exchange during the growing season of a permanently inundated fen, Agricultural and Forest Meteorology, 204, 94–105, https://doi.org/10.1016/j.agrformet.2015.02.002, https://linkinghub.elsevier.com/retrieve/pii/S0168192315000301, 2015.

Lafleur, P. M., Roulet, N. T., Bubier, J. L., Frolking, S., and Moore, T. R.: Interannual variability in the peatland-atmosphere carbon dioxide exchange at an ombrotrophic bog, Global Biogeochemical Cycles, 17, n/a–n/a, https://doi.org/10.1029/2002GB001983, http://doi.wiley.com/10.1029/2002GB001983, 2003.

Lapen, D. R., Price, J. S., and Gilbert, R.: Soil water storage dynamics in peatlands with shallow water tables, Canadian Journal of Soil Science, 80, 43–52, https://doi.org/10.4141/S99-007, http://www.nrcresearchpress.com/doi/10.4141/S99-007, 2000.

Lavendel, B.: Ecological Restoration in the Face of Global Climate Change: Obstacles and Initiatives, Ecological Restoration, 21, 199–203, http://www.jstor.org/stable/43440452, 2003.

Leifeld, J., Müller, M., and Fuhrer, J.: Peatland subsidence and carbon loss from drained temperate fens, Soil Use and Management, 27, 170–176, https://doi.org/10.1111/j.1475-2743.2011.00327.x, http://doi.wiley.com/10.1111/j.1475-2743.2011.00327.x, 2011.

Leipe, T. and Leipe, S.: Vegetation und Vogelwelt des Huetelmoores, Hansestadt Rostock. Abschluss-Bericht über eine zweijährige Bestand-serfassung (2016 und 2017)., Tech. rep., Rostock, 2017.

Limpens, J., Berendse, F., Blodau, C., Canadell, J. G., Freeman, C., Holden, J., Roulet, N., Rydin, H., and Schaepman-Strub, G.: Peatlands and the carbon cycle: from local processes to global implications – a synthesis, Biogeosciences, 5, 1475–1491, https://doi.org/10.5194/bg-5-1475-2008, http://www.biogeosciences.net/5/1475/2008/, 2008.

Lund, M., Christensen, T. R., Lindroth, A., and Schubert, P.: Effects of drought conditions on the carbon dioxide dynamics in a temperate peatland, Environmental Research Letters, 7, 045 704, https://doi.org/10.1088/1748-9326/7/4/045704, http://stacks.iop.org/1748-9326/7/i=4/a=045704?key=crossref.14f58d732cadbeedf921143dafe9536d, 2012.

Matthes, J. H., Sturtevant, C., Verfaillie, J., Knox, S., and Baldocchi, D.: Parsing the variability in CH 4 flux at a spatially heterogeneous wetland: Integrating multiple eddy covariance towers with high-resolution flux footprint analysis, Journal of Geophysical Research: Biogeosciences, 119, 1322–1339, https://doi.org/10.1002/2014JG002642, http://doi.wiley.com/10.1002/2014JG002642, 2014.

Moen, A., Hans, J., and Tanneberger, F.: Mires and peatlands of Europe. Status, distribution and conservation., Schweizerbart Science Publishers, Stuttgart, Germany, http://www.schweizerbart.de//publications/detail/isbn/9783510653836/Joosten_Tanneberger_Moen_Mires_and_peat, 2017.

Montgomery, R. B.: Vertical eddy flux of heat in the atmosphere, Journal of Meteorology, 5, 265–274, https://doi.org/10.1175/1520-0469(1948)005<0265:VEFOHI>2.0.CO;2, http://journals.ametsoc.org/doi/abs/10.1175/1520-0469%281948%29005%3C0265%3AVEFOHI%3E2.0.CO%3B2, 1948.

Pachauri, R. K., Allen, M. R., Barros, V. R., Broome, J., Cramer, W., Christ, R., Church, J. A., Clarke, L., Dahe, Q., Dasgupta, P., Dubash, N. K., Edenhofer, O., Elgizouli, I., Field, C. B., Forster, P., Friedlingstein, P., Fuglestvedt, J., Gomez-Echeverri, L., Hallegatte, S., Hegerl, G., Howden, M., Jiang, K., Jimenez Cisneroz, B., Kattsov, V., Lee, H., Mach, K. J., Marotzke, J., Mastrandrea, M. D., Meyer, L., Minx, J., Mulugetta, Y., O'Brien, K., Oppenheimer, M., Pereira, J. J., Pichs-Madruga, R., Plattner, G. K., Pörtner, H. O., Power, S. B., Preston, B., Ravindranath, N. H., Reisinger, A., Riahi, K., Rusticucci, M., Scholes, R., Seyboth, K., Sokona, Y., Stavins, R., Stocker, T. F., Tschakert, P., van Vuuren, D., and van Ypserle, J. P.: Climate Change 2014: Synthesis Report. Contribution of Working Groups I, II and III to the Fifth Assessment Report of the Intergovernmental Panel on Climate Change, Tech. rep., https://doi.org/10013/epic.45156.d001, https://epic.awi.de/id/eprint/37530/, 2014.

390   Pfadenhauer, J. and Grootjans, A.: Wetland restoration in Central Europe: aims and methods, Applied Vegetation Science, 2, 95–106, https://doi.org/10.2307/1478886, http://doi.wiley.com/10.2307/1478886, 1999.

Riutta, T., Laine, J., and Tuittila, E.-S.: Sensitivity of CO2 Exchange of Fen Ecosystem Components to Water Level Variation, Ecosystems, 10, 718–733, https://doi.org/10.1007/s10021-007-9046-7, http://link.springer.com/10.1007/s10021-007-9046-7, 2007.

Shurpali, N. J., Verma, S. B., Kim, J., and Arkebauer, T. J.: Carbon dioxide exchange in a peatland ecosystem, Journal of Geophysical
395   Research, 100, 14 319, https://doi.org/10.1029/95JD01227, http://doi.wiley.com/10.1029/95JD01227, 1995.

Steffenhagen, P., Zak, D., Schulz, K., Timmermann, T., and Zerbe, S.: Biomass and nutrient stock of submersed and floating macrophytes in shallow lakes formed by rewetting of degraded fens, Hydrobiologia, 692, 99–109, https://doi.org/10.1007/s10750-011-0833-y, http://link.springer.com/10.1007/s10750-011-0833-y, 2012.

Sulman, B. N., Desai, A. R., Saliendra, N. Z., Lafleur, P. M., Flanagan, L. B., Sonnentag, O., Mackay, D. S., Barr, A. G., and van der Kamp,
400   G.: CO 2 fluxes at northern fens and bogs have opposite responses to inter-annual fluctuations in water table, Geophysical Research Letters, 37, n/a–n/a, https://doi.org/10.1029/2010GL044018, http://doi.wiley.com/10.1029/2010GL044018, 2010.

Tiemeyer, B., Freibauer, A., Borraz, E. A., Augustin, J., Bechtold, M., Beetz, S., Beyer, C., Ebli, M., Eickenscheidt, T., Fiedler, S., Förster, C., Gensior, A., Giebels, M., Glatzel, S., Heinichen, J., Hoffmann, M., Höper, H., Jurasinski, G., Laggner, A., Leiber-Sauheitl, K., Peichl-Brak, M., and Drösler, M.: A new methodology for organic soils in national greenhouse gas inventories: Data synthesis, derivation and
405   application, Ecological Indicators, 109, 105 838, https://doi.org/10.1016/j.ecolind.2019.105838, https://linkinghub.elsevier.com/retrieve/pii/S1470160X19308325, 2020.

Timmermann, T., Joosten, H., and Succow, M.: Restaurierung von Mooren, in: Renaturierung von Ökosystemen in Mitteleuropa, edited by Zerbe, S. and Wiegleb, G., chap. Restaurier, pp. 55–93, Spektrum Akademischer Verlag, Heidelberg, https://doi.org/10.1007/978-3-8274-2161-6, http://link.springer.com/10.1007/978-3-8274-2161-6, 2009.

410   van Diggelen, R., Middleton, B., Bakker, J., Grootjans, A., and Wassen, M.: Fens and floodplains of the temperate zone: Present status, threats, conservation and restoration, Applied Vegetation Science, 9, 157, https://doi.org/10.1658/1402-2001(2006)9[157:fafott]2.0.co;2, 2006.

Wang, H., Richardson, C. J., and Ho, M.: Dual controls on carbon loss during drought in peatlands, Nature Climate Change, 5, 584–587, https://doi.org/10.1038/nclimate2643, http://www.nature.com/articles/nclimate2643, 2015.

415   Yu, Z., Loisel, J., Brosseau, D. P., Beilman, D. W., and Hunt, S. J.: Global peatland dynamics since the Last Glacial Maximum, Geophysical Research Letters, 37, n/a–n/a, https://doi.org/10.1029/2010GL043584, http://doi.wiley.com/10.1029/2010GL043584, 2010.